Synthesis, Breathing, and Gas Sorption Study of the First Isoreticular Mixed-Linker Phosphonate Based Metal-Organic Frameworks

Marco Taddei, Ferdinando Costantino, Andrea Ienco, Angiolina Comotti, Phuong V. Dau and Seth M. Cohen

Electronic Supplementary Information

Chemicals.

Copper acetate monohydrate was purchased from Carlo Erba Reagenti. All the other chemicals were purchased from Sigma-Aldrich.

Synthesis of the phosphonic acids.

N,N,N'N'-tetrakis(phosphonomethyl)-α,α'-*p*-xylylenediamine (H_8L^1) and N,N,N'N'-tetrakis(phosphonomethyl)hexamethylenediamine (H_8L^2) were synthesized according to the Moedritzer-Irani method: the diamine (15 mmol) and the phosphorus acid (60 mmol) were dissolved in 30 mL of HCl 6 M and the solution was refluxed. Paraformaldehyde (120 mmol) was dispersed in a little amount of water and was added in small portions in 3 hours. The solvent was then evaporated under vacuum and the residue was treated with ethanol. A white solid formed and was filtered under vacuum. This solid was recrystallized from H_2O. Yield: 82% for H_8L^1, 74% for H_8L^2.

^{1}H-NMR (D_2O+K_2CO_3, 400 MHz): H_8L^1: δ = 7.63 (s, 4H, aromatic), 4.71 (d, 4H, Ph-CH_2-N), 3.35 (d, 8H, N-CH_2-P) ppm; H_8L^2: δ= 3.43 (t, 4H, CH_2-CH_2-$\underline{CH_2}$-N), 3.23 (d, 8H, N-CH_2-P), 1.73 (m, 4H, CH_2-$\underline{CH_2}$-CH_2-N), 1.37 (m, 4H, $\underline{CH_2}$-CH_2-CH_2-N) ppm.

^{31}P-NMR (D_2O+K_2CO_3, 400 MHz): H_8L^1: δ= 8.15 (m) ppm; H_8L^2: δ= 7.83 (m) ppm.

Synthesis of $Cu_3(H_2L^1)(bipy)_2 \cdot 9H_2O$ (1).

1 was prepared as follows: in a 100 mL Erlenmeyer flask, 0.25 mmol of copper acetate monohydrate and 0.375 mmol of bipy were dissolved in 100 mL of water, then 0.125 mmol of H_8L^1 were added. A light blue powder immediately formed and the mixture was kept under stirring for 30 minutes. The flask was then put inside an oven at 80 °C to slowly evaporate the solution. After one day, when the volume of solution had reduced to about 30 mL, the powder had turned into deep blue single crystals, which were filtered under vacuum and washed with water. The crystals were stable upon standing at air.

85 mg of product were recovered. Yield: 88.0% (calculated on Cu).

Analysis: Calcd. for $Cu_3P_4C_{32}N_6O_{21}H_{52}$: Cu = 16.44%, P = 10.69%; Exp: Cu = 15.72%, P = 9.37%.

Synthesis of $Cu_3(H_2L^2)(bipy)_2 \cdot 6H_2O$ (2_*np*).

2 was prepared as follows: in a 100 mL Erlenmeyer flask, 0.25 mmol of copper acetate monohydrate and 0.375 mmol of bipy were dissolved in 100 mL of water, then 0.125 mmol of H_8L^2 were added. A light blue powder immediately formed and the mixture was kept under stirring for 30 minutes. The flask was then put inside an oven at 80 °C to slowly evaporate the solution. After one day, when the volume of solution had reduced to about 30 mL, the powder had turned into blue single crystals, which were filtered under vacuum and washed with water. The crystals (**2**_*lp* phase) lost water upon standing at air and underwent phase transition, turning into powder (**2**_*np* phase).

91 mg of product were recovered. Yield: 99.6% (calculated on Cu).

Analysis: Calcd. for $Cu_3P_4C_{30}N_6O_{18}H_{50}$: Cu = 17.38%, P = 11.30%; Exp: Cu = 15.53%, P = 11.55%.

Synthesis of $Cu_3(H_2L^2)(etbipy)_2 \cdot 9H_2O$ (3_*np*).

3 was prepared as follows: in a 250 mL Erlenmeyer flask, 0.75 mmol of copper acetate monohydrate and 1.125 mmol of etbipy were dissolved in 250 mL of water, then 0.375 mmol of H_8L^2 were added. A light blue powder immediately formed and the mixture was kept under stirring for 30 minutes. The flask was then put inside an oven at 80 °C to slowly evaporate the solution. After one day, when the volume of solution had reduced to about 150 mL, 100 mL of water were added and the mixture was left reacting for another day. When the volume had reduced to 150 mL again, the powder had completely turned into blue single crystals, which were filtered under vacuum and washed with water. The crystals (**3**_*lp* phase) lost water upon standing at air and underwent phase transition, turning into powder (**3**_*np* phase).

194 mg of product were recovered. Yield: 64.3% (calculated on Cu).

Analysis: Calcd. for $Cu_3P_4C_{34}N_6O_{21}H_{64}$: Cu = 15.80%, P = 10.28%; Exp: Cu = 16.43%, P = 9.17%.

Analytical methods.

Elemental Analysis. The copper and phosphorus contents of samples were obtained by inductively coupled plasma optical emission spectroscopy using a Varian Liberty Series II instrument working in axial geometry, after mineralization of the samples with a mixture of concentrated hydrochloric acid and concentrated nitric acid.

Single Crystal Diffraction. Tables S1-S4 report the crystal data of **1**, **2**_*lp*, **3**_*lp*, and **3**_*np* respectively. Single crystals of **2**_*lp*, **3**_*lp*, and **3**_*np* taken from H_2O were mounted on nylon loops with paratone oil and placed under a nitrogen cold stream. The data of **1**, **2**_*lp*, and **3**_*np* were collected at low temperature (100 K for **1** and 150 K for **2**_*lp* and **3**_*np*) on an Oxford Diffraction Xcalibur diffractometer equipped with Cu-Kα radiation (λ = 1.54180 Å). Data of **3**_*lp* was collected at 200 K on a Bruker Apex diffractometer using Mo-Kα (λ = 0.71073 Å) radiation controlled using the APEX 2010 software package. A multi-scan method utilizing equivalents was employed to correct for absorption. All the structures were solved by direct methods and refined to convergence by full-matrix least squares against F^2 using all data with *SHELXL-97*. All structures were treated with the "SQUEEZE" protocol in *PLATON* to account for partially occupied or disordered solvent (e.g. H_2O) within the porous framework.

Crystallographic data (excluding structure factors) for the compounds reported in this paper have been deposited with the Cambridge Crystallographic Data Centre as supplementary publication CCDC 909973, 909974, 909975 and 909976 for **1**, **2**_*lp*, **3**_*lp*, and **3**_*np*, respectively. Copies of the data can be obtained free of charge on application to CCDC, 12 Union Road, Cambridge CB2 1EZ, UK (fax: (+44) 1223-336-033; email: deposit@ccdc.cam.ac.uk).

Powder X-Ray Diffraction. PXRD patterns were collected with a PANalytical X'PERT PRO diffractometer equipped with a X'Celerator solid state fast detector in the 5-35 2θ range and with a 40 s/step counting time. The PXRD pattern of **2**_*np* for the Le Bail fitting was collected in the 4-80 2θ range and with a 60 s/step counting time. The model-biased Le Bail fit was performed by using the *GSAS* program, placing one copper atom in the centre of the unit cell and refining 29 parameters (unit cell, background, and profile function).

Thermogravimetric Analysis. TGA were performed using a Netzsch STA490C thermoanalyzer under a 20 mL min^{-1} air flux with a heating rate of 5° C min^{-1}.

BET Surface Area and Gas Sorption Analysis. ~30-100 mg of MOF material was evacuated under vacuum for a minimum of ~3 h at 120 ^{o}C. Samples were then transferred to a pre-weighed sample tube and degassed at 105 °C on a Micromeritics ASAP 2020 Adsorption Analyzer for a minimum of 12 h or until the outgas rate was <5 mmHg/min. The sample tube was re-weighed to obtain a consistent mass for the degassed MOF. Brunauer-Emmett-Teller (BET) surface area (m^2/g) measurements were collected at 77 K with N_2 on a Micromeritics ASAP 2020 Adsorption Analyzer using a volumetric technique. The samples were then manually degassed for at least 2 h prior to N_2 and CO_2 isotherm.

High pressure volumetric CO_2 measurements were performed up to 10 bar and 298 K with a Micromeritics ASAP 2050. A known weight of the compounds, typically 200 mg, was placed into a sample tube, then the change of the pressure was monitored and the degree of adsorption was measured by the decrease of the pressure at the equilibrium state.

Table S1. Crystal data and structure refinement for **1**.

Empirical formula	C32 H38 Cu3 N6 O14 P4
Formula weight	1045.17
Temperature	100(2) K
Wavelength	1.5418 Å
Crystal system /Space group	Triclinic; P-1
Unit cell dimensions	a = 9.4686(9) Å.
	b = 11.8434(9) Å.
	c = 12.3923(10) Å.
	α= 117.656(9)°.
	β= 94.288(8)°.
	γ = 97.946(7)°.
Volume	1203.70(18) $Å^3$
Z	1
Density (calculated)	1.439 Mg/m^3
Absorption coefficient	3.333 mm^{-1}
F(000)	529
Crystal size	0.22 x 0.18 x 0.05 mm^3
Theta range for data collection	4.27 to 72.61°.
Index ranges	-10<=h<=11, -14<=k<=14, -15<=l<=15
Reflections collected	15935
Independent reflections	4723 [R(int) = 0.0728]
Completeness to theta = 72.61°	98.7 %
Absorption correction	Semi-empirical from equivalents
Max. and min. transmission	1 and 0.48664
Refinement method	Full-matrix least-squares on F^2
Data / restraints / parameters	4723 / 0 / 268
Goodness-of-fit on F^2	1.031
Final R indices [I>2sigma(I)]	R1 = 0.0606, wR2 = 0.164
R indices (all data)	R1 = 0.0865, wR2 = 0.1916
Largest diff. peak and hole	0.769 and -0.887 e.$Å^{-3}$

Table S2. Crystal data and structure refinement for **2**_*lp*.

Empirical formula	C30 H38 Cu3 N6 O12 P4
Formula weight	989.16
Temperature	150(2) K
Wavelength	1.5418 Å
Crystal system, Space group	Triclinic, P-1
Unit cell dimensions	a = 9.5516(5) Å.
	b = 12.9047(7) Å.
	c = 13.982(2) Å.
	α= 75.544(7)°.
	β= 89.628(7)°.
	γ = 75.697(5)°.
Volume	1614.3(3) $Å^3$
Z	1
Density (calculated)	1.017 Mg/m^3
Absorption coefficient	2.437 mm^{-1}
F(000)	503
Crystal size	0.15 x 0.08 x 0.06 mm^3
Theta range for data collection	4.24 to 62.07°.
Index ranges	-10<=h<=10, -14<=k<=14, -15<=l<=15
Reflections collected	9346
Independent reflections	4899 [R(int) = 0.0523]
Completeness to theta = 62.07°	96.5 %
Absorption correction	Semi-empirical from equivalents
Max. and min. transmission	1 and 0.83577
Refinement method	Full-matrix least-squares on F^2
Data / restraints / parameters	4899 / 0 / 250
Goodness-of-fit on F^2	1.352
Final R indices [I>2sigma(I)]	R1 = 0.1101, wR2 = 0.2669
R indices (all data)	R1 = 0.1324, wR2 = 0.2774

Table S3. Crystal data and structure refinement for **3**_*lp*.

Empirical formula	C34 H50 Cu3 N6 O12 P4
Formula weight	1045.22
Temperature	200(2) K
Wavelength	0.71073 Å
Crystal system, Space group	Monoclinic, P21/n
Unit cell dimensions	a = 13.9010(4) Å
	b = 9.5384(3) Å
	c = 26.6923(12) Å.
	α= 90°.
	β= 96.326(3)°.
	γ = 90°.
Volume	3517.7(2) $Å^3$
Z	2
Density (calculated)	0.981 Mg/m^3
Absorption coefficient	1.029 mm^{-1}
F(000)	1058
Crystal size	0.05 x 0.05 x 0.03 mm^3
Theta range for data collection	1.54 to 21.93°.
Index ranges	-14<=h<=14, -9<=k<=10, -26<=l<=28
Reflections collected	6431
Independent reflections	3816 [R(int) = 0.0299]
Completeness to theta = 21.93°	89.3 %
Absorption correction	Semi-empirical from equivalents
Max. and min. transmission	0.9137 and 0.8345
Refinement method	Full-matrix least-squares on F^2
Data / restraints / parameters	3816 / 3 / 258
Goodness-of-fit on F^2	1.113
Final R indices [I>2sigma(I)]	R1 = 0.0774, wR2 = 0.2284
R indices (all data)	R1 = 0.0899, wR2 = 0.2392
Largest diff. peak and hole	0.876 and -0.565 $e.Å^{-3}$

Table S4. Crystal data and structure refinement for **3**_*np*.

Empirical formula	C34 H48 Cu3 N6 O13 P4
Formula weight	1063.27
Temperature	100(2) K
Wavelength	1.5418 Å
Crystal system, Space group	Monoclinic, P 21/c
Unit cell dimensions	a = 23.288(2) Å.
	b = 9.5700(7) Å.
	c = 24.207(2) Å.
	α= 90°.
	β= 105.705(9)°.
	γ = 90°.
Volume	5193.5(7) $Å^3$
Z	4
Density (calculated)	1.357 Mg/m^3
Absorption coefficient	3.081 mm^{-1}
F(000)	2172
Crystal size	0.2 x 0.18 x 0.02 mm^3
Theta range for data collection	4.73 to 61.88°.
Index ranges	-25<=h<=25, -10<=k<=10, -26<=l<=27
Reflections collected	17869
Independent reflections	7908 [R(int) = 0.0653]
Completeness to theta = 61.88°	97.1 %
Absorption correction	Semi-empirical from equivalents
Max. and min. transmission	1 and 0.18913
Refinement method	Full-matrix least-squares on F^2
Data / restraints / parameters	7908 / 0 / 541
Goodness-of-fit on F^2	1.035
Final R indices [I>2sigma(I)]	R1 = 0.1024, wR2 = 0.273
R indices (all data)	R1 = 0.1316, wR2 = 0.2991

Figures Referenced in the Manuscript.

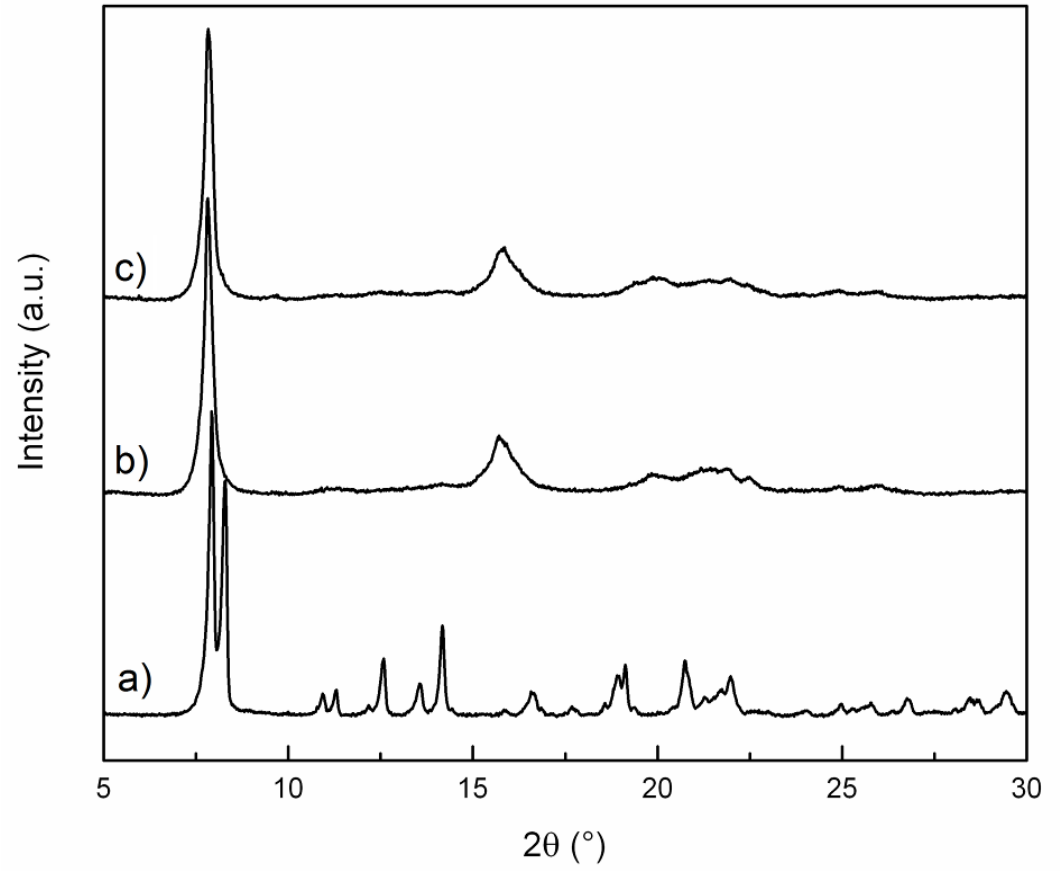

Figure S1. PXRD patterns of **1** as-synthesized (a), at 120 °C (b), and at RT after thermal treatment (c).

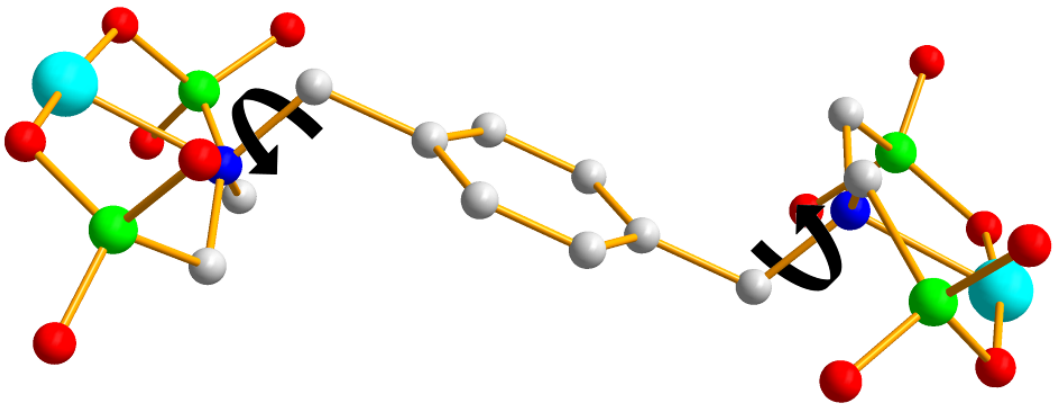

Figure S2. The rotational degrees of freedom of the L^1 ligand in **1**.

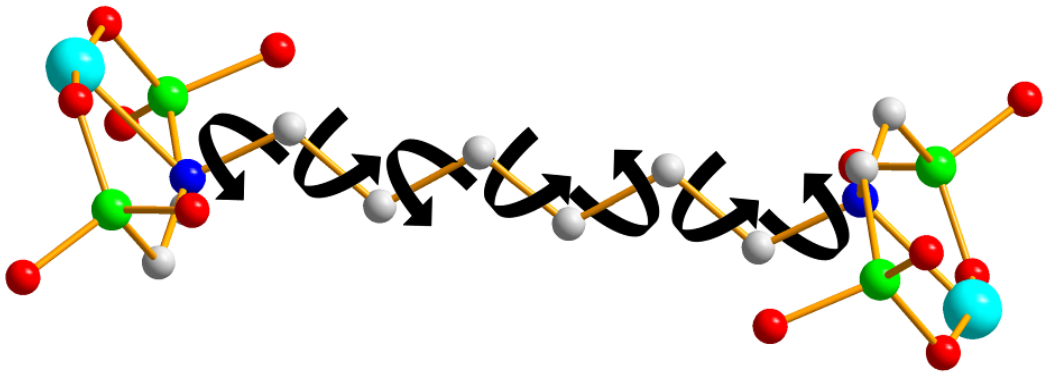

Figure S3. The rotational degrees of freedom of the L^2 ligand in **2** and in **3**.

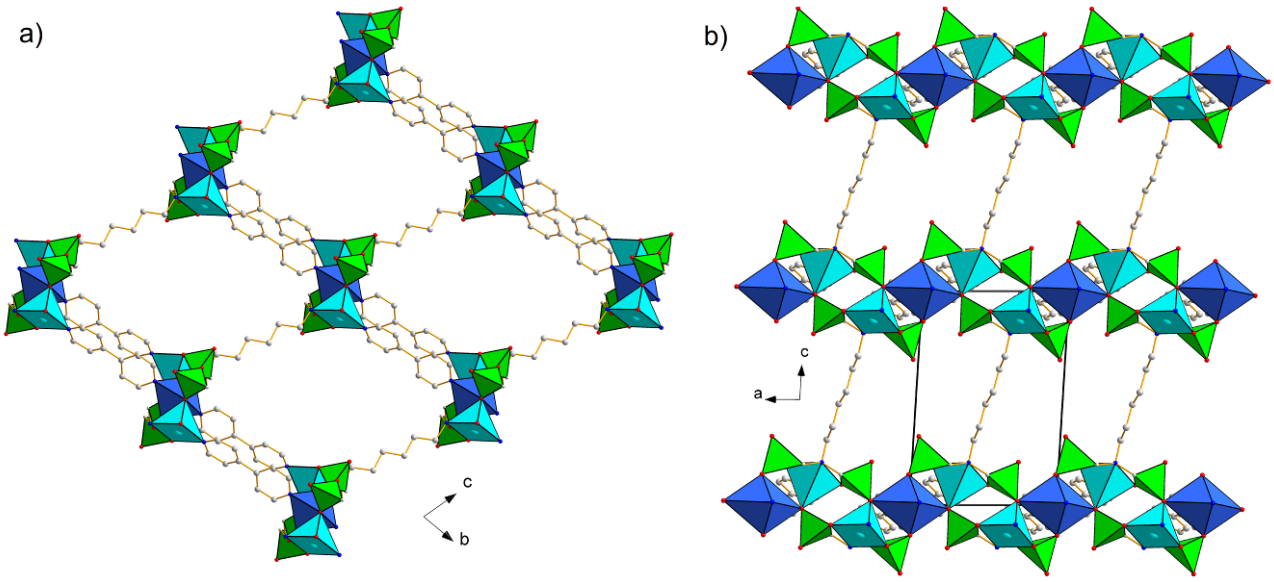

Figure S4. View of the structure of **2**_*lp* along the *a* axis (a) and parallel to the same axis (b).

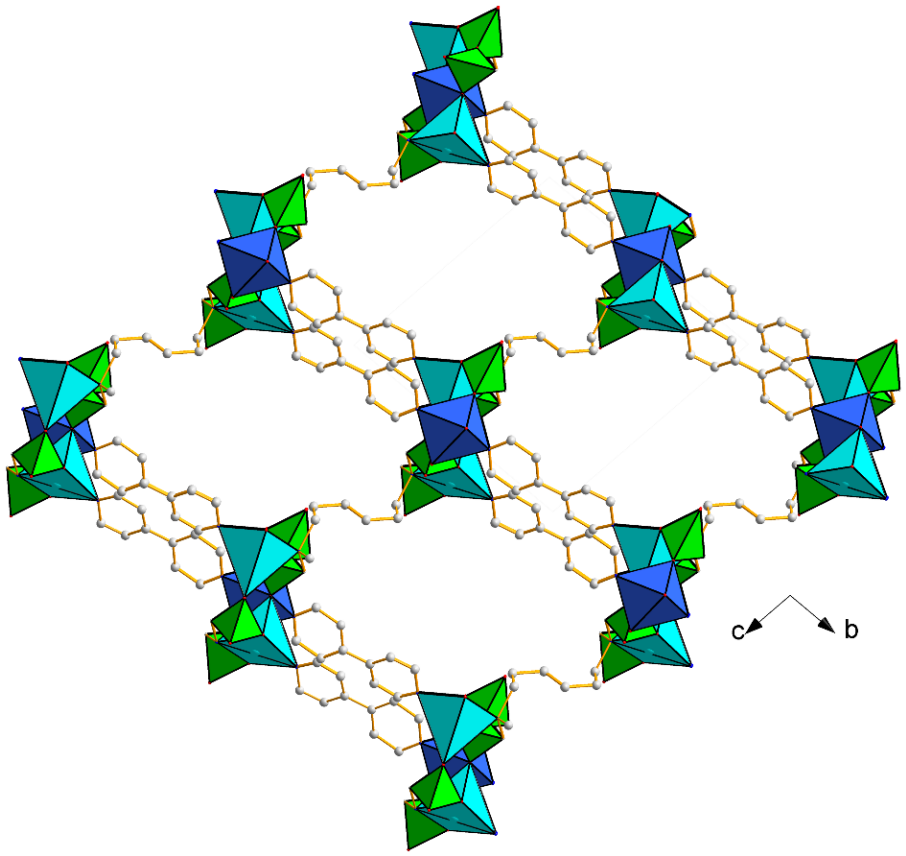

Figure S5. Proposed model of the structure of **2**_*np*, based on the structure of **2**_*lp*.

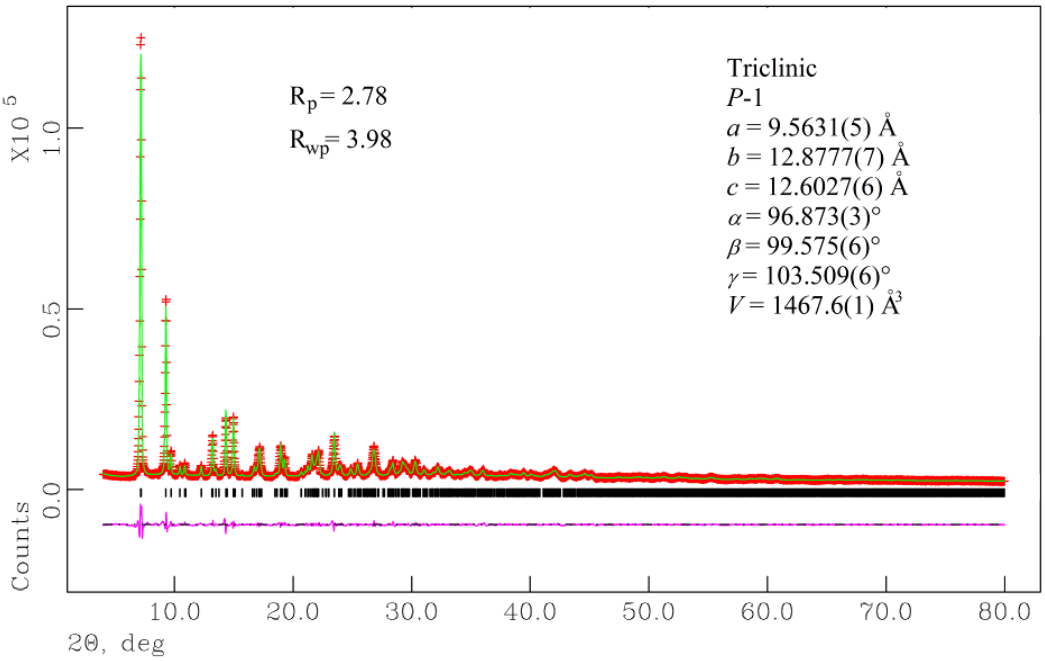

Figure S6. Plot of the Le Bail fit on the PXRD pattern of **2**_*np*. The final R values and refined unit cell parameters are reported.

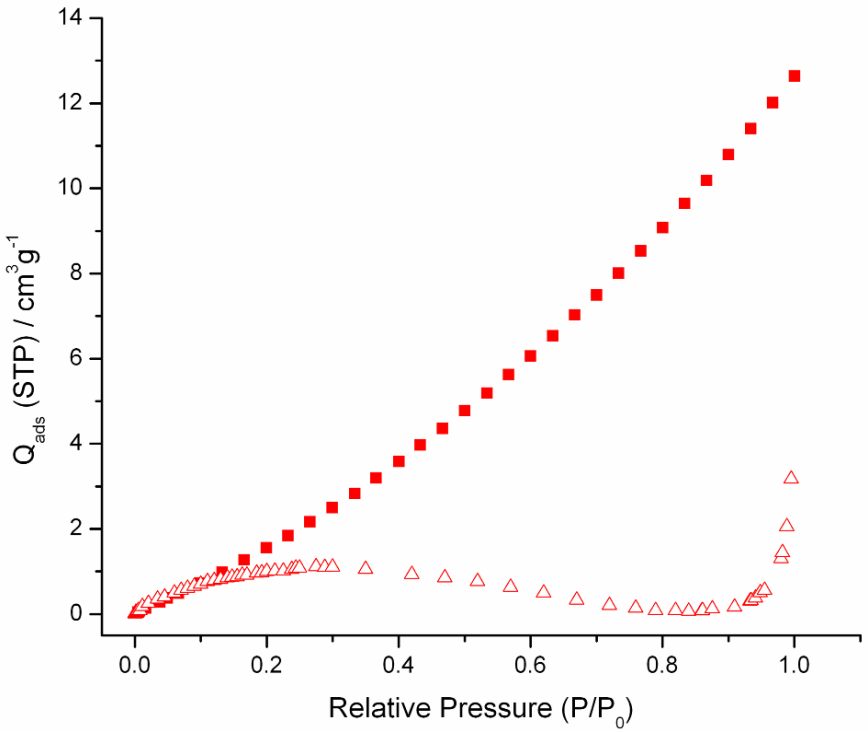

Figure S7. N_2 (open triangles) and CO_2 (solid squares) adsorption isotherms (195 K) measured for **1**.

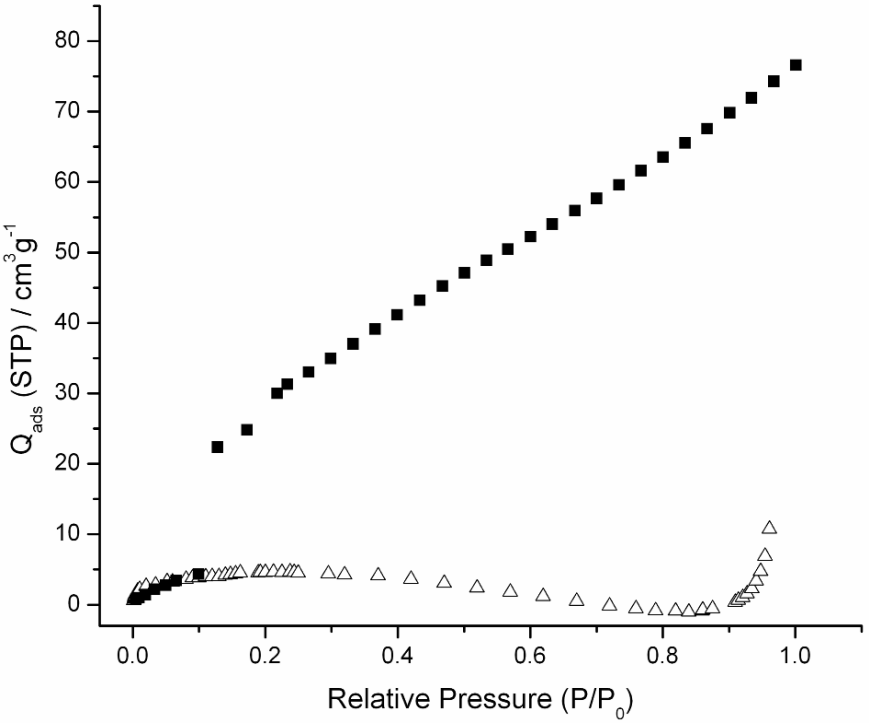

Figure S8. N_2 (open triangles) and CO_2 (solid squares) adsorption isotherms (195 K) measured for **2**.

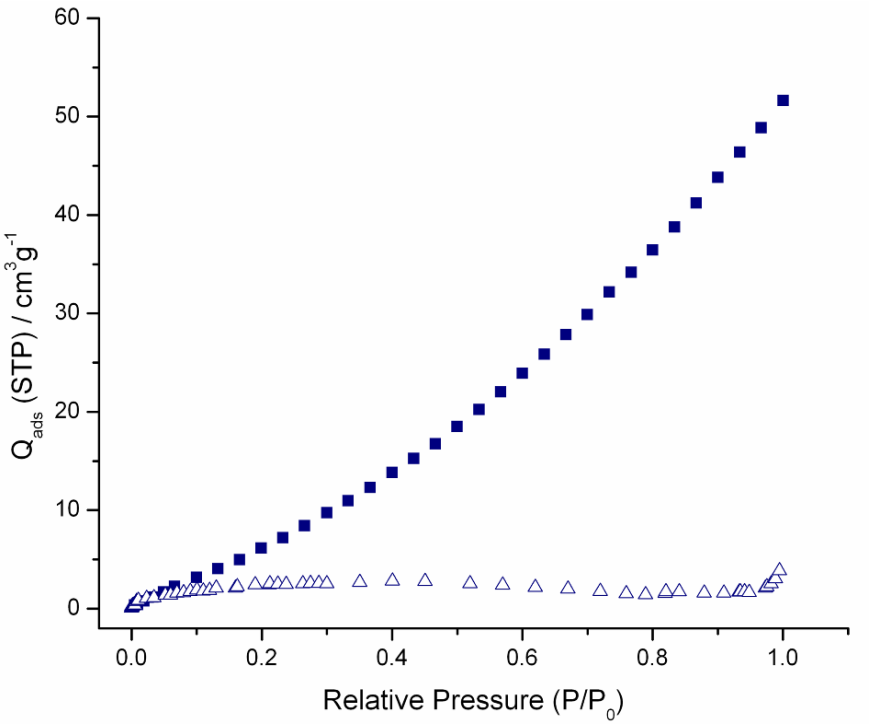

Figure S9. N_2 (open triangles) and CO_2 (solid squares) adsorption isotherms (195 K) measured for **3**.

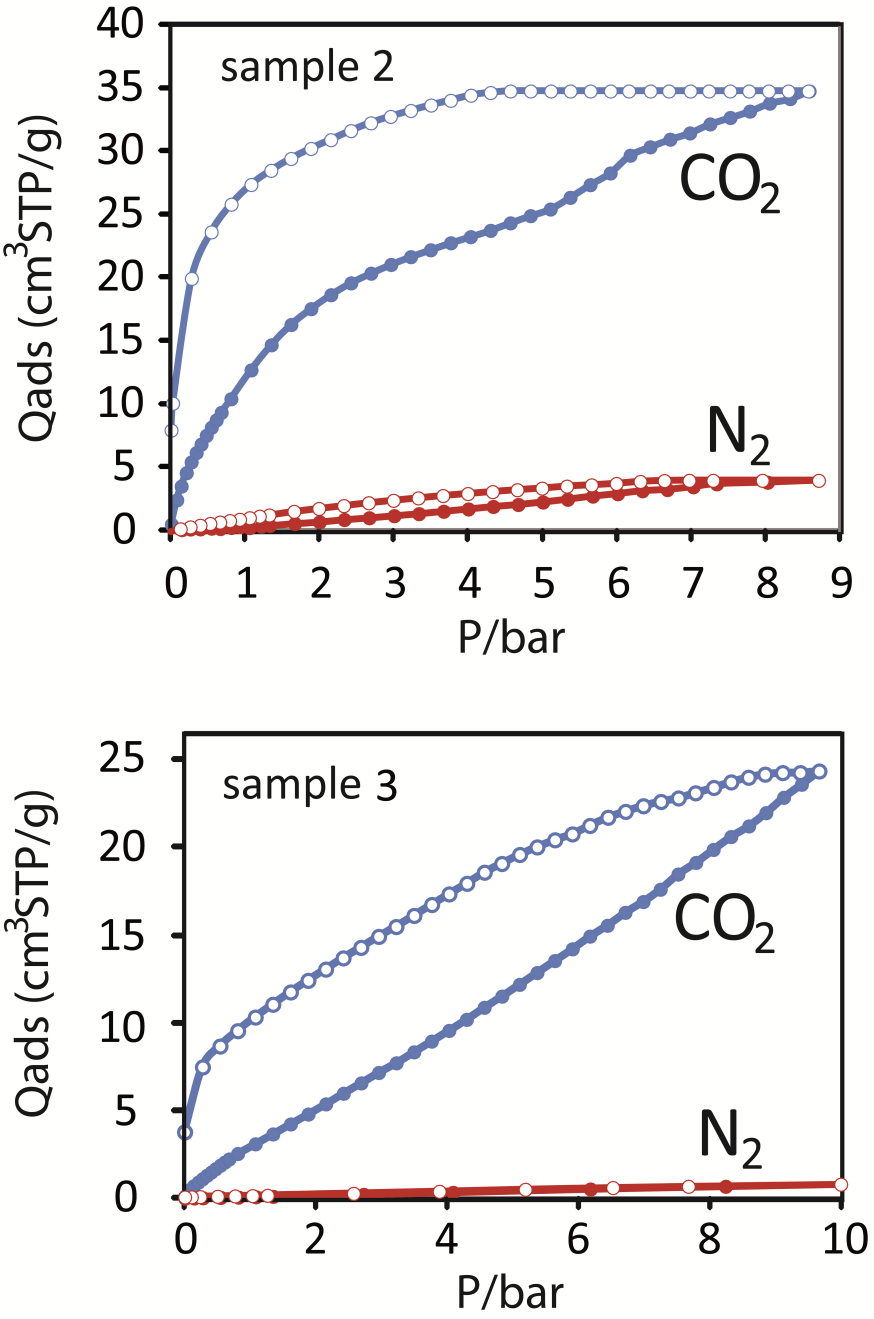

Figure S10. High pressure (10 bar) CO_2 adsorption (blue, solid circles) and desorption (blue, open circles) isotherms (298 K) and N_2 adsorption (red, solid circles) and desorption (red, open circles) isotherms (298 K) measured for **2** and **3**. Negligible amounts of CO_2 and N_2 uptake have been detected by the isotherms of sample **1** (not shown).

Additional Structure Pictures.

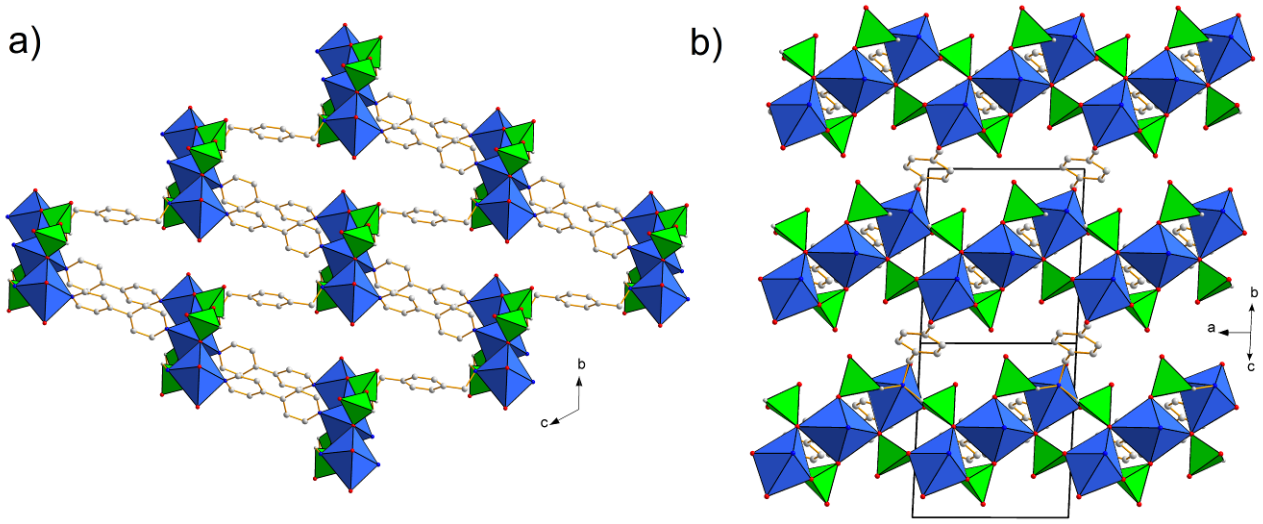

Figure S11. View of the structure of **1** along the *a* axis (a) and parallel to the same axis (b).

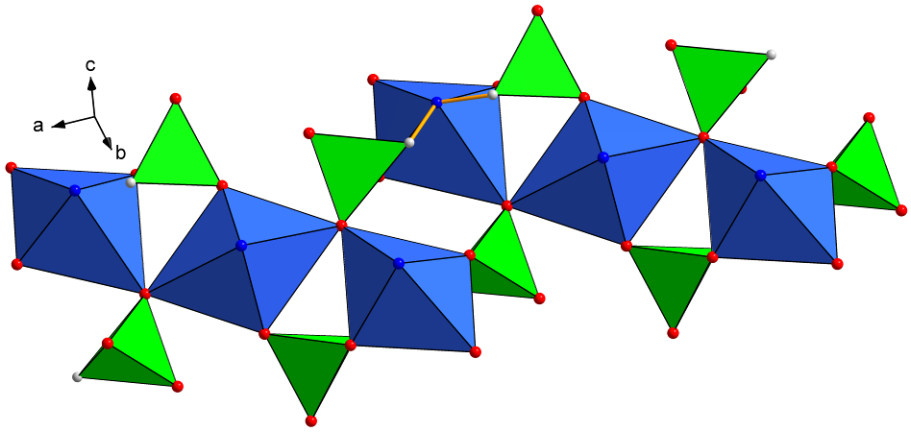

Figure S12. Polyhedral representation of the copper-phosphonate CBU of **1.**

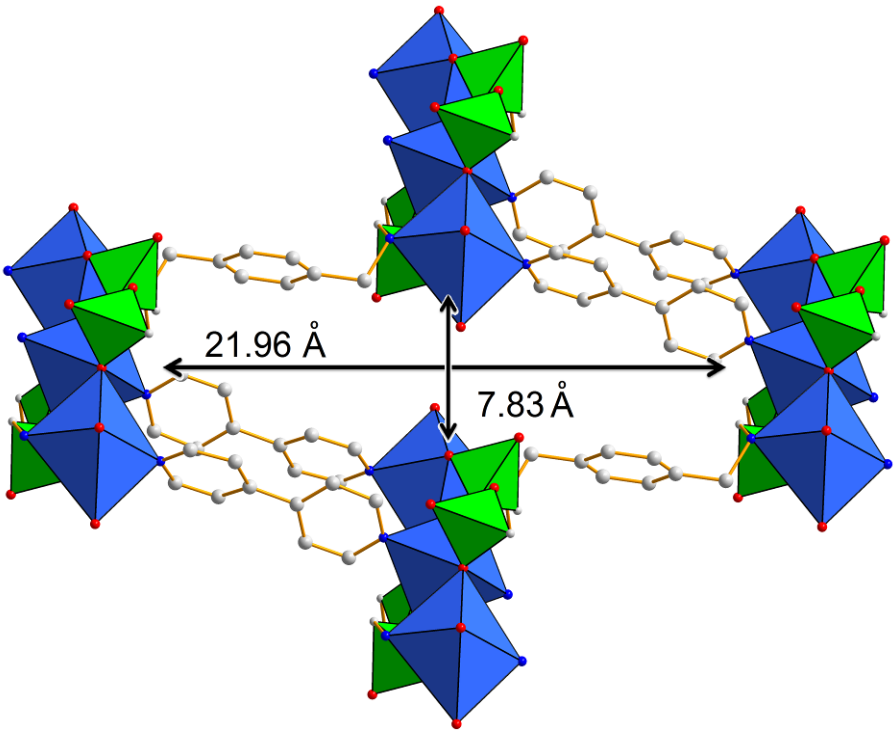

Figure S13. View of one channel of **1**.

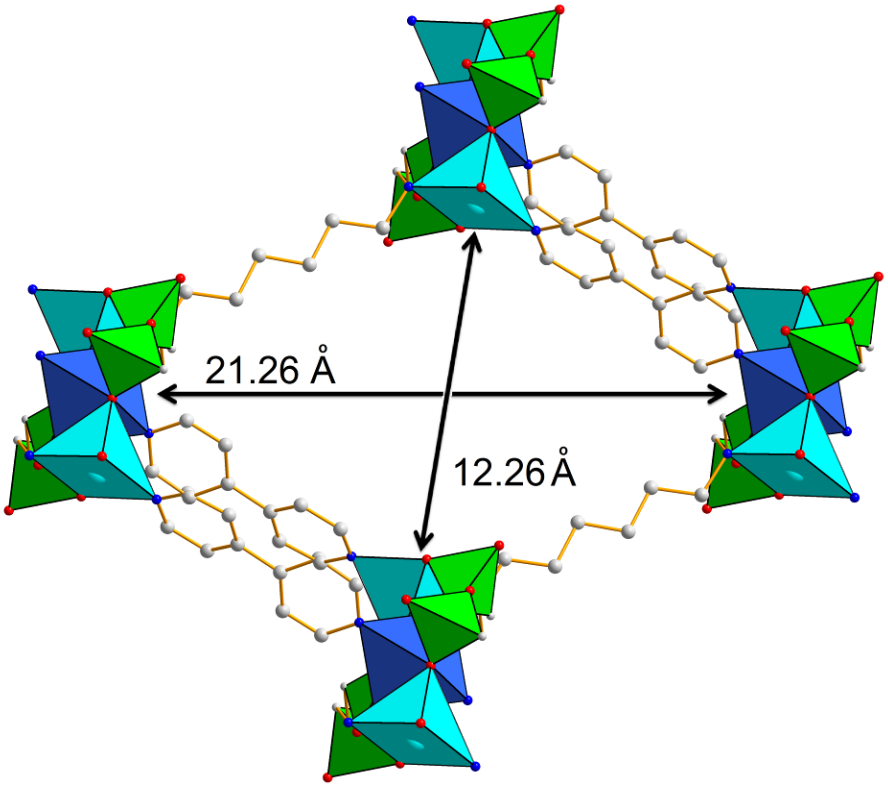

Figure S14. View of one channel of **2**_*lp*.

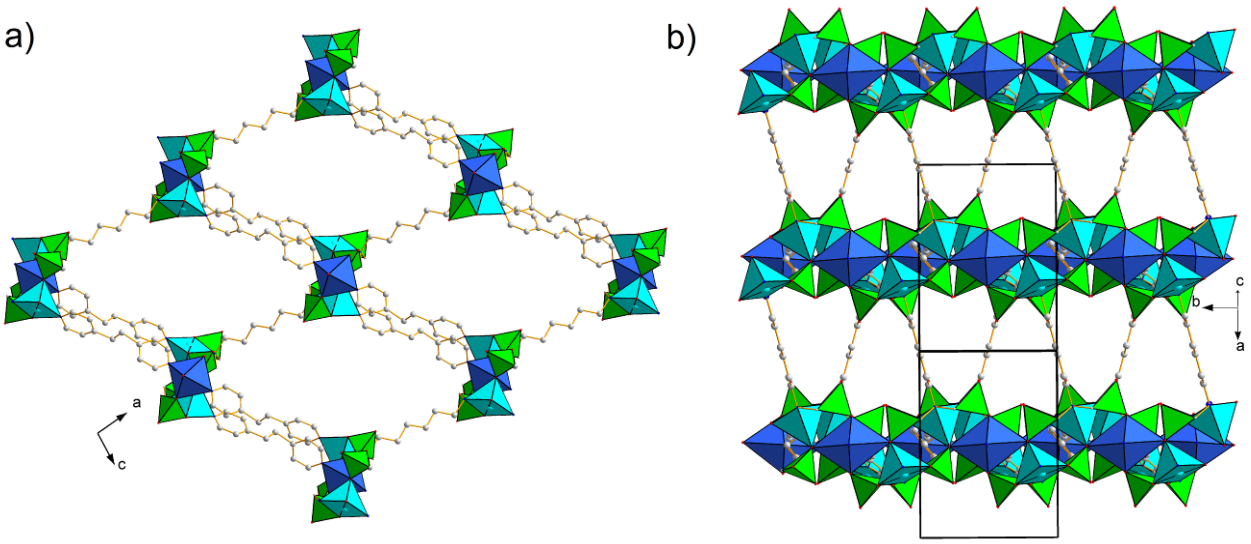

Figure S15. View of the structure of **3**_*lp* along the *b* axis (a) and parallel to the same axis (b).

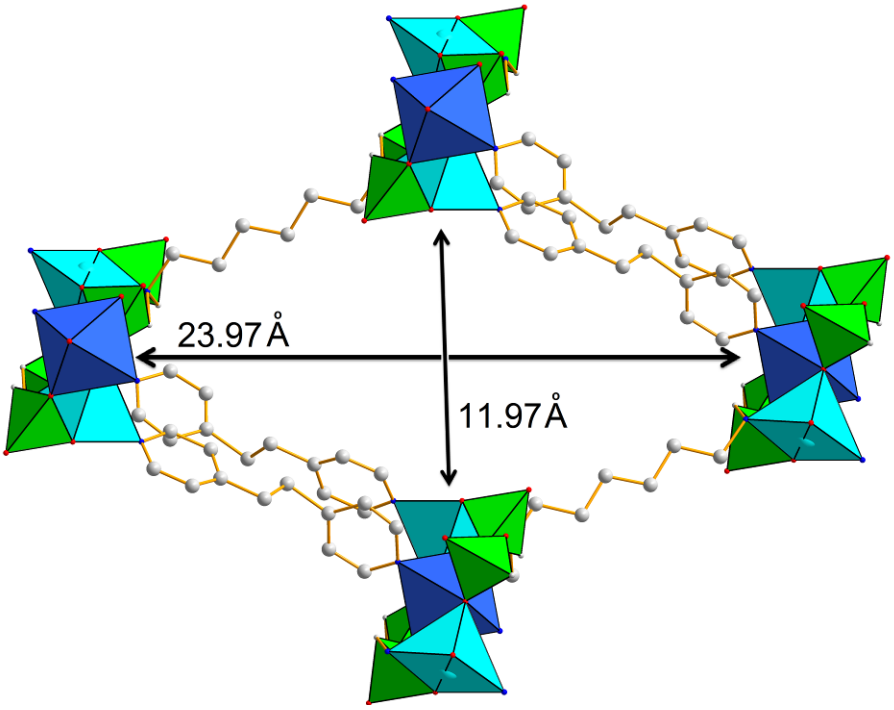

Figure S16. View of one channel of **3**_*lp*.

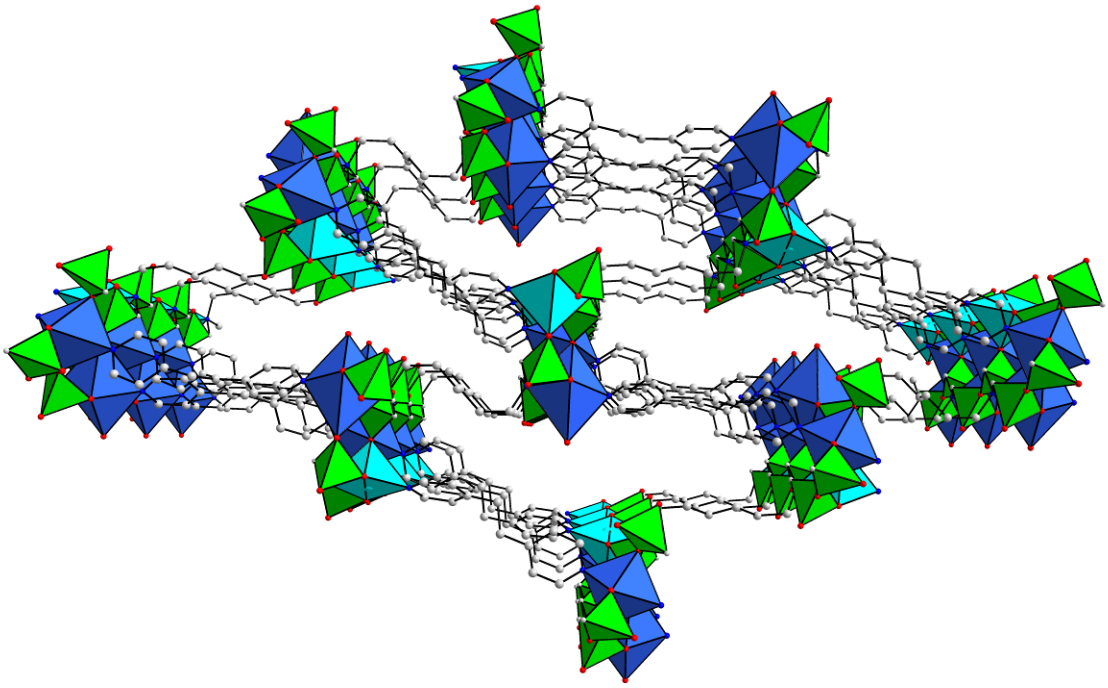

Figure S17. View of the structure of **3**_*np* along the *b* axis.

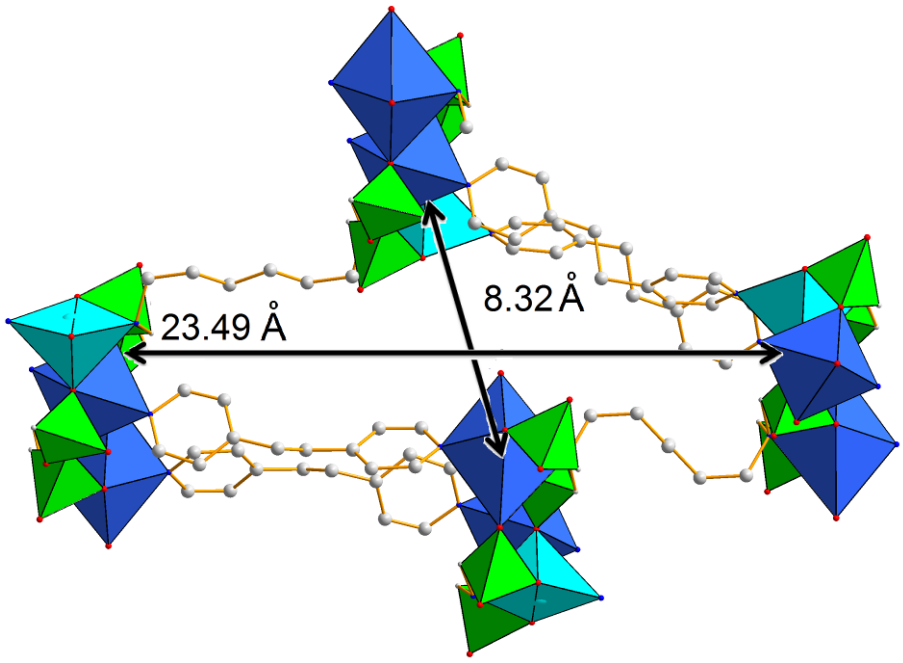

Figure S18. View of one channel of **3**_*np*.

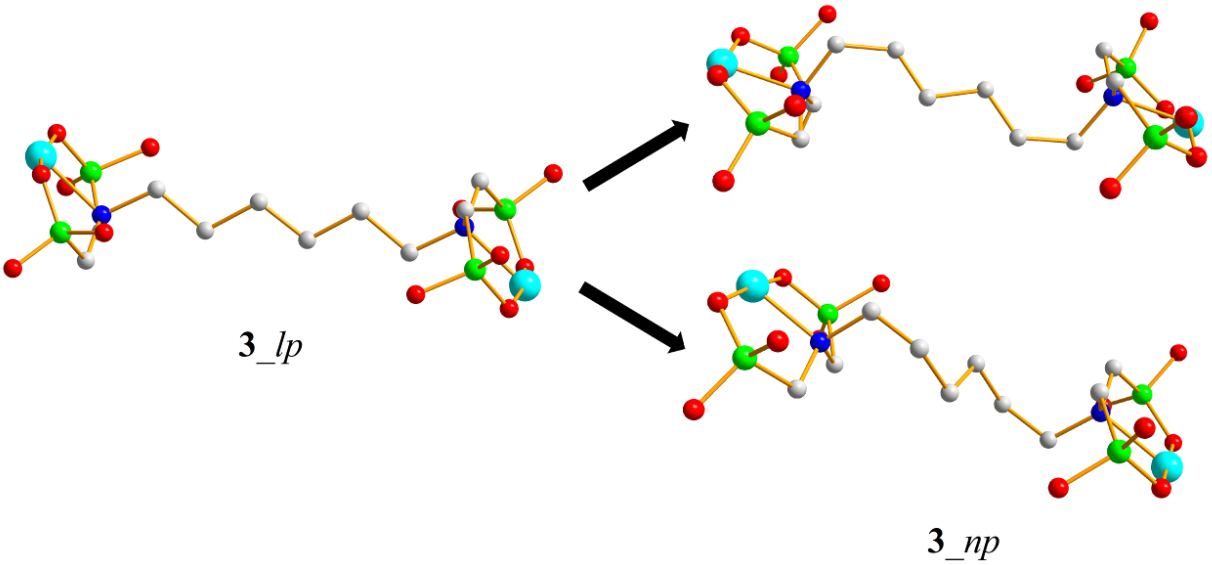

Figure S19. Conformational change of the alkyl chain of the L^2 ligand in the **3**_*lp* to **3**_*np* transition.

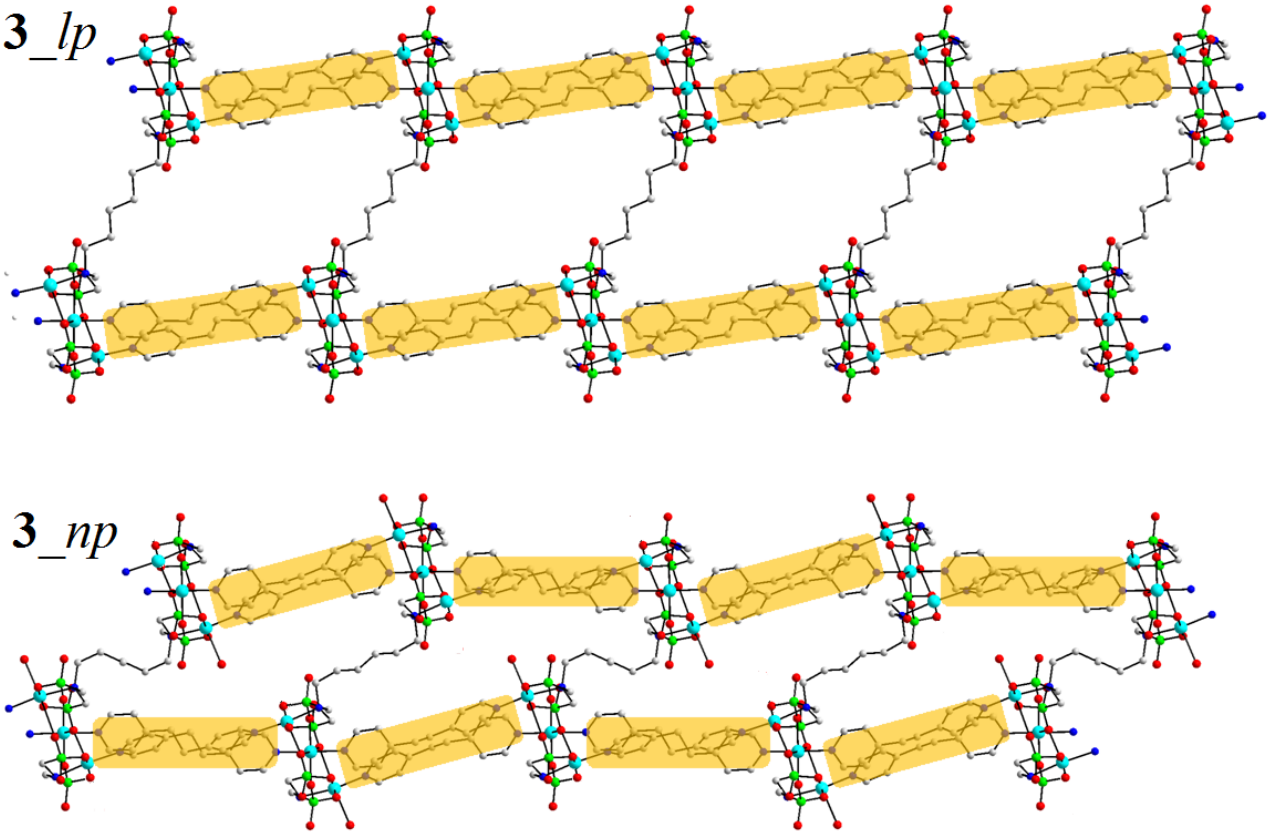

Figure S20. Rearrangement of the layers defined by the inorganic chains and the bipyridines associated with the transition from **3**_*lp* to **3**_*np*.

Hydration Effects.

The effects of the different degrees of hydration in **1**, **2** and **3** were studied with PXRD.

The structure of **1** shows no significant rearrangements in dependence of the amount of water contained inside the channels. The TG analysis of the compound (Figure S21) shows that it loses 12.2% of its weight around 100 °C. This value corresponds to about 3 water molecules per copper atom. After this weight loss the compound is stable up to about 250 °C, when decomposition of the organic part begins. The final weight loss at 1200 °C is 55.2%.

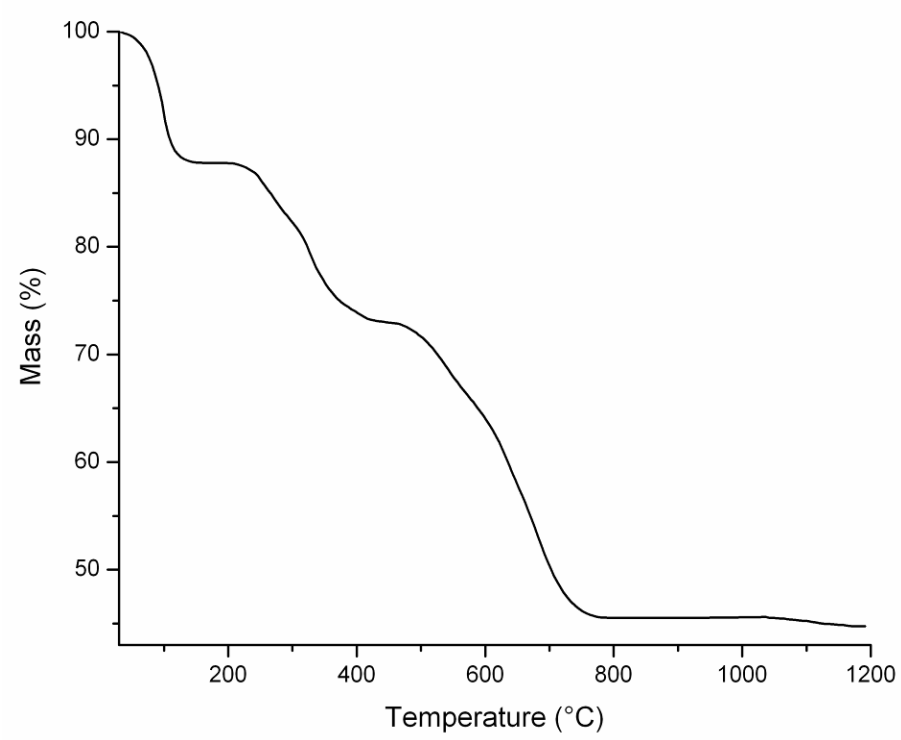

Figure S21. TG curve of **1**.

Figure S1 reports the comparison of the PXRD spectra at room temperature, 120 °C and room temperature after thermal treatment. The compound loses crystallinity as the temperature is raised, and at 120 °C only a few reflections are still visible. The most prominent effect is the shift towards lower 2θ value and superposition of the first two reflections (001 and 010), indicating that, upon

losing water, the structure stretches a little. When the compound is cooled to room temperature, no significant modifications in the diffraction pattern take place, suggesting that water cannot get back into the structure. This could be justified taking into account the relative rigidity of the L^1 ligand, which possesses only two possible rotational degrees of freedom, as shown in Figure S2.

On the contrary, the structural rearrangements observed in **2** can be basically related to the high number of possible conformations of the six-carbon alkyl chain of the phosphonic ligand (Figure S3). The study of the transition between the **2**_*lp* and the **2**_*np* phase by means of PXRD is reported in Figure S22.

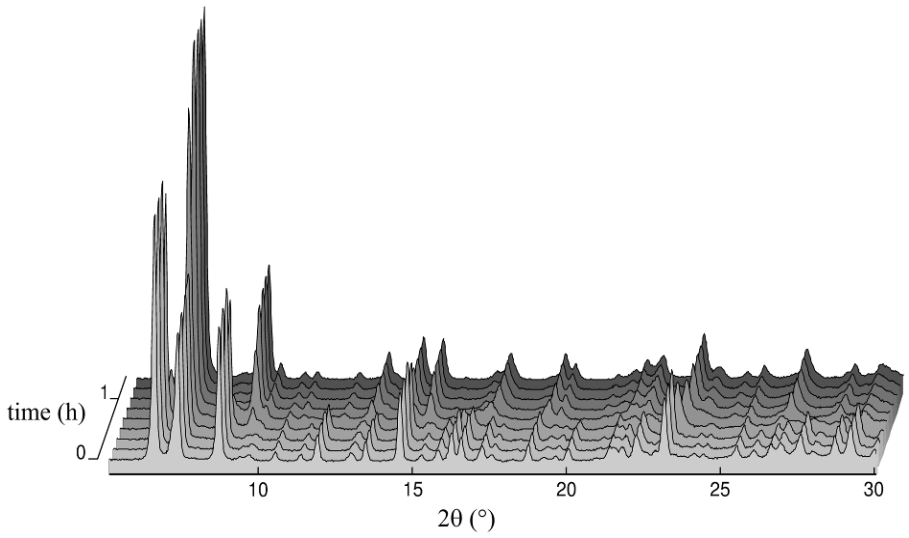

Figure S22. Time dependent PXRD plot describing the **2**_*lp* to **2**_*np* transition.

The PXRD spectra were recorded in continuous on a freshly synthesized sample, which was filtered under vacuum and immediately deposited on a flat sample holder in order to follow the dehydration process. At the beginning, the pattern is perfectly superimposable with that simulated for the structure of the **2**_*lp* phase obtained from single crystal data; the transition to the **2**_*np* phase occurs quite fast without formation of intermediate phases. The most evident effect is the shift of the 001 reflection from 6.5° to 7.2°, thus overlapping with the 010 reflection: this behavior is in agreement

with the reduced length of the *c* axis, which changes from 13.982 in the **2**_*lp* phase to 12.603 in the **2**_*np* phase. On the other hand, the *a* and *b* axes remain substantially the same, suggesting that no modifications occur in the plane defined by the inorganic chains and the bipyridines. Notably, the transition from the **2**_*lp* to the **2**_*np* phase is not reversible: by putting the **2**_*np* phase in water at room temperature and analyzing the evolution of the structure with X-rays, it can be observed that it is not possible to get back to the **2**_*lp* phase, though some structural modifications take place. The 001 reflection shifts towards lower 2θ values, but the value of 6.5°, typical of the **2**_*lp,* is not reproduced, even if the compound is held in water for many hours.

The TG analysis of the **2**_*np* phase (Figure S23) shows a 10% weight loss around 100 °C: it can be ascribed to the loss of the water molecules held in the channels. The number of water molecules calculated from this weight loss is two per copper atom. After this weight loss the compound is stable up to about 250 °C, when decomposition of the organic part begins. The final weight loss at 1200 °C is 53%.

To calculate the number of water molecules in the **2**_*lp* phase, we made the following assumptions: the volume difference between the unit cells of the two phases is solely due to the different water content and the volume of a single water molecule is about 30 $Å^3$. The volume difference is 147 $Å^3$ (1614 $Å^3$ for **2**_*lp*, 1467 $Å^3$ for **2**_*np*) , that means the unit cell of **2**_*lp* contains five water molecules more than that of **2**_*np*.

The presence of a stable phase between 100 and 200°C pushed us to investigate the high temperature behavior of this material. Figure S24 reports the comparison of the PXRD spectra at room temperature, 120 °C and room temperature after thermal treatment.

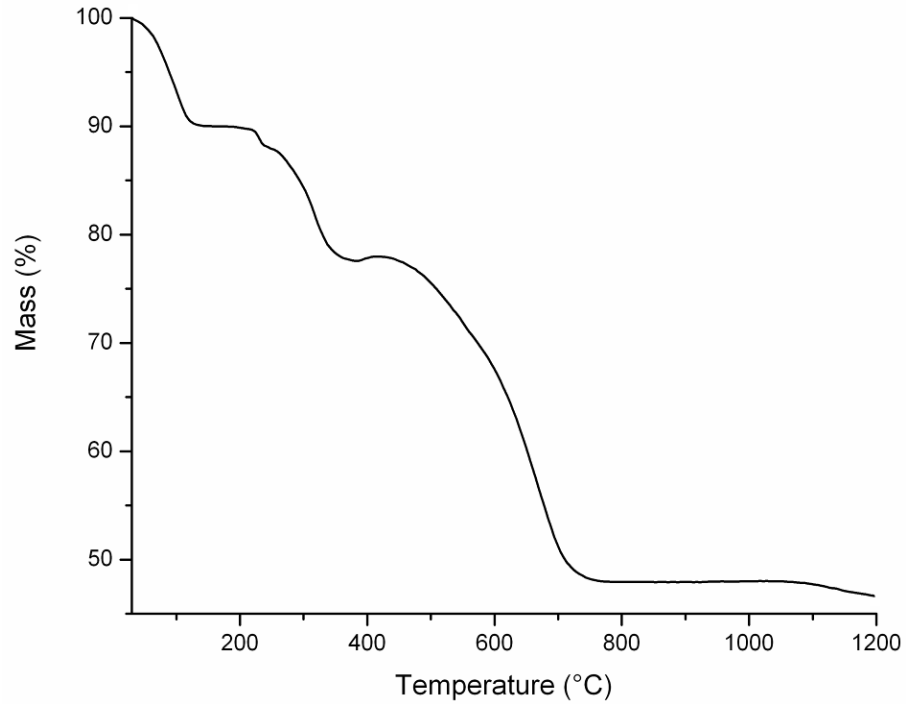

Figure S23. TG curve of **2**_*np*.

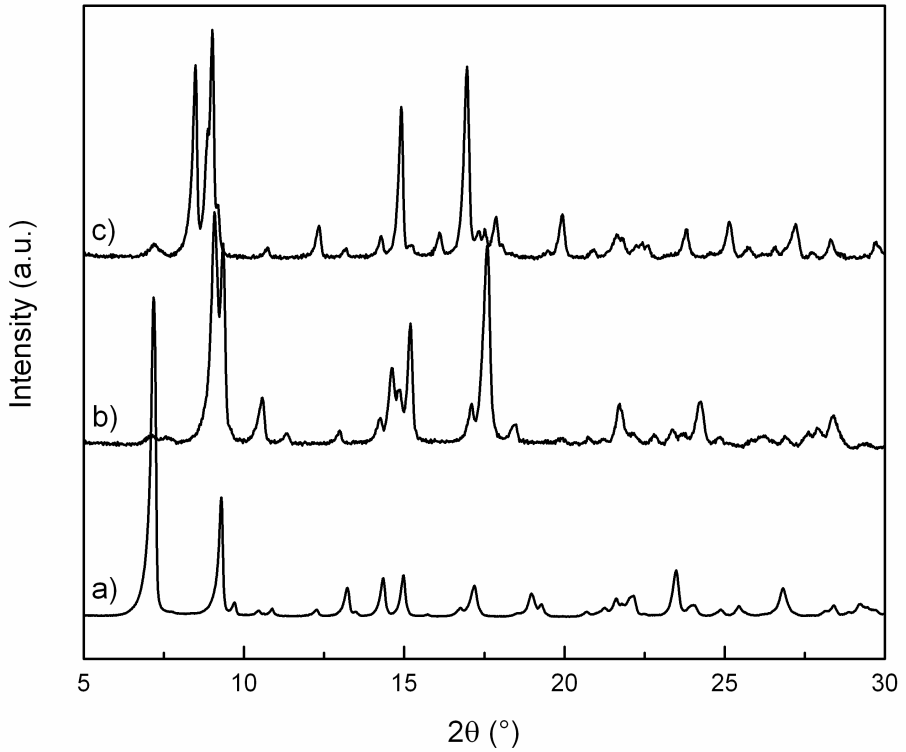

Figure S24. PXRD patterns of **2**_*np* (a), when heated at 120 °C (b), and at RT after thermal treatment (c).

It can be seen that there is a shift of many reflections towards higher 2θ values, indicating a general shrinkage of the structure. Once the compound is brought back to room temperature, it is not able to adopt the initial structure of the **2**_*np* phase, also if kept at moist air for relatively long times, indicating that very likely it cannot absorb water from the atmosphere. Conversely, the **2**_*np* phase can be regenerated if the compound is kept in water for some hours and then dried at room temperature.

The behavior of **3** is much more complex and interesting, suggesting that the major flexibility and length of etbipy compared to bipy allow an increased number of possible conformations of the structure. In this case, the transition from **3**_*lp* to **3**_*np* is reversible and very easy: by simply wetting the **3**_*np* phase of this compound, a shifting towards lower 2θ values of many peaks in the diffraction pattern can be observed, and the resulting profile is very similar, even if not exactly superimposable, with the simulated pattern of the **3**_*lp* phase solved from single crystal data. Figure S25 shows a series of diffraction patterns acquired in continuous in order to follow the *lp*-to-*np* transition at room temperature: here the transition is slower and more gradual than in **2**, and the pure **3**_*np* phase is formed after five hours from the wetting of the sample.

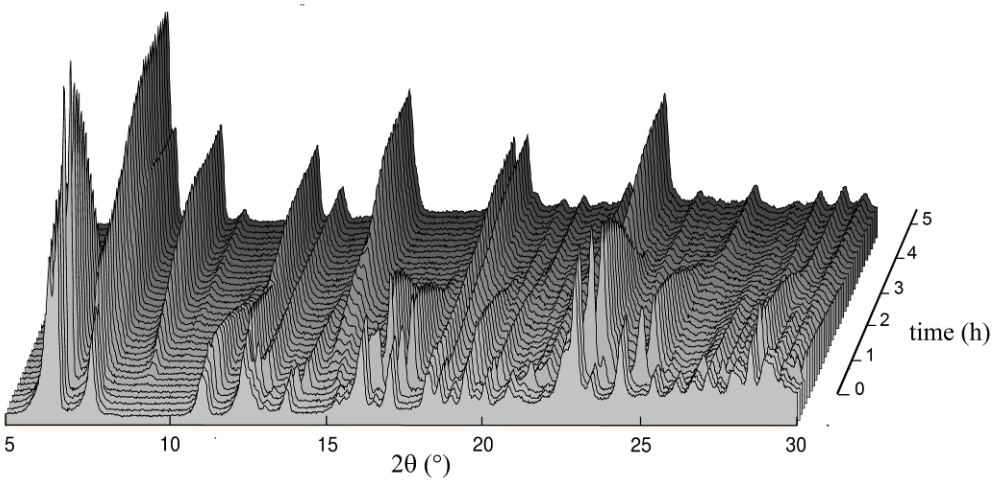

Figure S25. Time dependent PXRD plot describing the **3**_*lp* to **3**_*np* transition.

The TG analysis (Figure S26) of the **3**_*np* phase shows a 14% weight loss around 100 °C: as in the other compounds, it can be ascribed to the loss of water molecules held inside the channels. The calculated number of water molecules is about 3 per copper atom. After the first weight loss, the compound is stable up to about 200 °C, when decomposition of the organic part of the framework occurs. The final weight loss at 1200 °C is 58.81%.

To calculate the number of water molecules in the **3**_*lp* phase, we made the same assumptions as for **2**; since the unit cells of **3**_*np* and **3**_*lp* are not directly comparable, due to the different cell arrangements deriving from the higher degree of disorder in **3**_*np*, we considered the volume associated with each copper atom for estimating the water content: for **3**_*lp* this volume is 586.3 $Å^3$ (V = 3518 $Å^3$, 6 Cu atoms per unit cell), whereas for **3**_*np* it is 432.8 $Å^3$ (V = 5194 $Å^3$, 12 Cu atoms per unit cell). Hence, the volume difference is 154 $Å^3$, corresponding to about five water molecules per copper atom.

As for **2**, we investigated the high temperature behavior of **3**. Figure S27 reports the comparison of the PXRD spectra at room temperature, 120 °C and room temperature after heating.

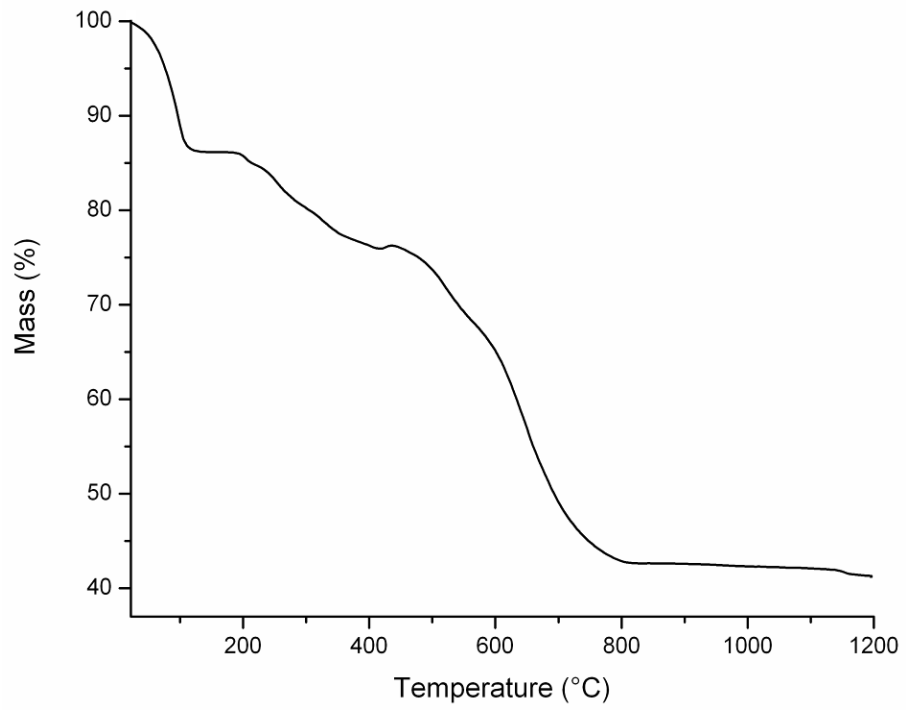

Figure S26. TG curve of **3**_*np*.

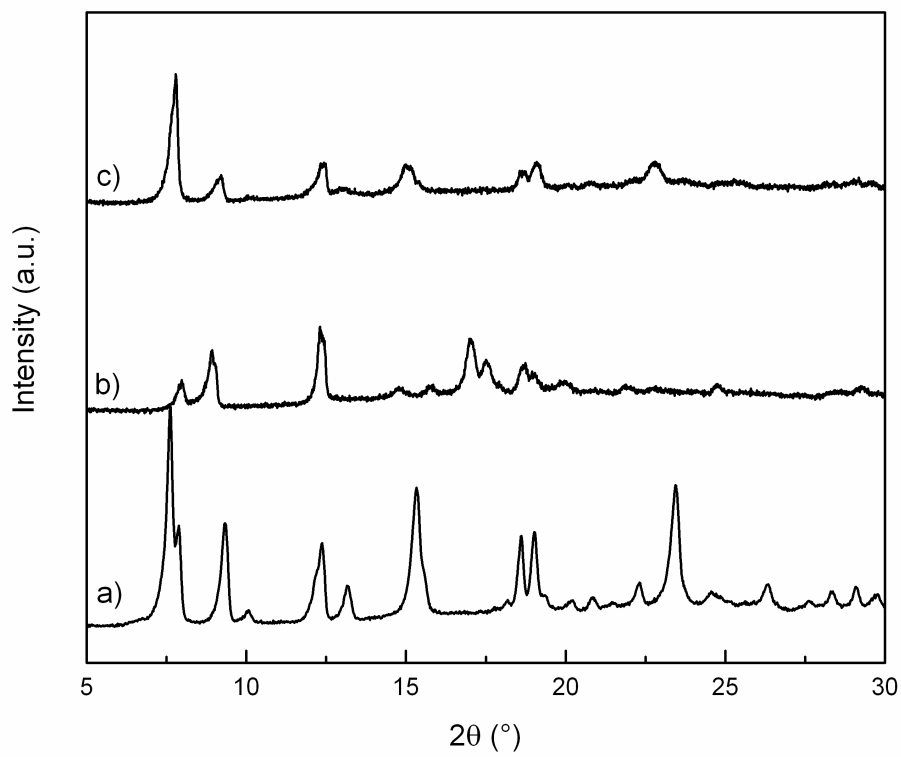

Figure S27. PXRD patterns of **3**_*np* (a), when heated at 120 °C (b), and at RT after thermal treatment (c).

The compound loses crystallinity as the temperature rises, and a general shrinkage of the structure can be deduced from the shifting towards higher 2θ values of most of the reflections. If the compound is allowed to cool at room temperature and left standing for many hours, it rearranges to a phase quite similar to the stable **3**_*np* phase, although the overall crystallinity is worse and some reflections are not matching. The TG analysis shows that the amount of water and the final weight loss of this new phase (hereafter called **3**_*np**) are the same as the **3**_*np* phase. If the **3**_*np** phase is kept in water for a short time and left drying at room temperature, a new phase (hereafter called **3**_*lp**) is obtained: this phase does not tend to lose as many water molecules as the **3**_*lp*, and is stable at room temperature, as shown by the PXRD pattern in Figure S28.

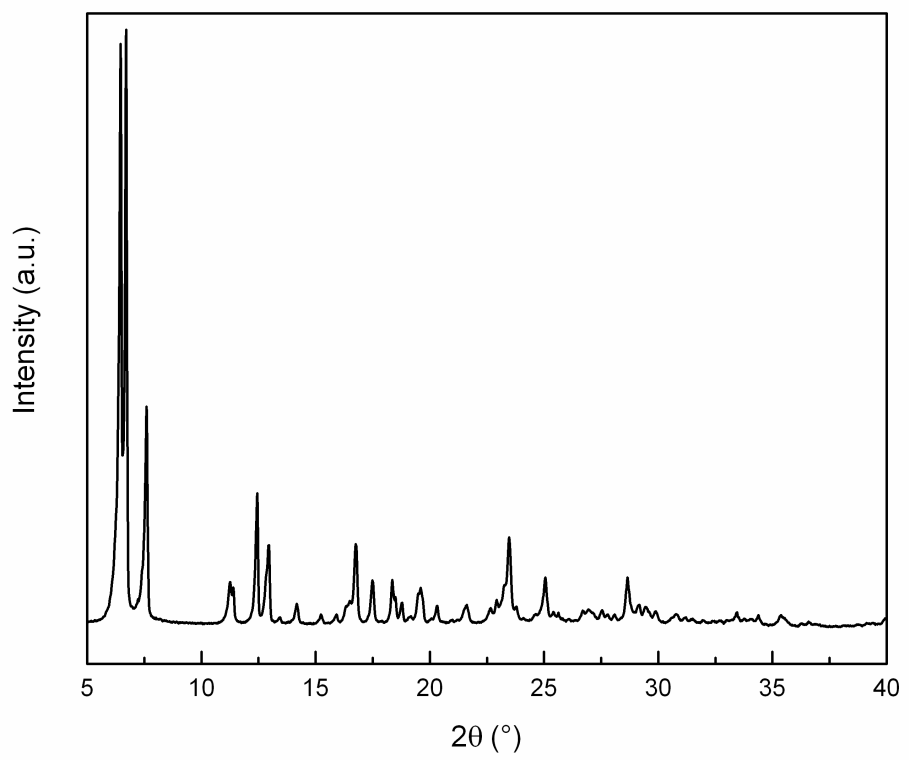

Figure S28. PXRD pattern of **3**_*lp**.

This pattern was indexed by a *P* 2_1/n monoclinic cell with the following lattice parameters: a = 27.67427 Å; b = 9.59050 Å; c = 13.96067 Å; β = 98.9575°; V = 3660.11 Å^3 (M_{20} = 12). The volume of this phase is even larger than that of **3**_*lp*. The TG analysis (Figure S29) of this phase shows a 19.72% weight loss occurring around 100 °C, indicating that a larger amount of water than in **3**_*np* is retained inside the framework. Assuming that the asymmetric unit is not affected by the thermal treatment, the amount of water calculated for this phase is about 5.3 per copper atom. This behavior may be explained admitting that the high temperature treatment of the starting **3**_*np* phase causes structural rearrangements that increase the rigidity of the framework, thus allowing the formation of the stable **3**_*lp** phase.

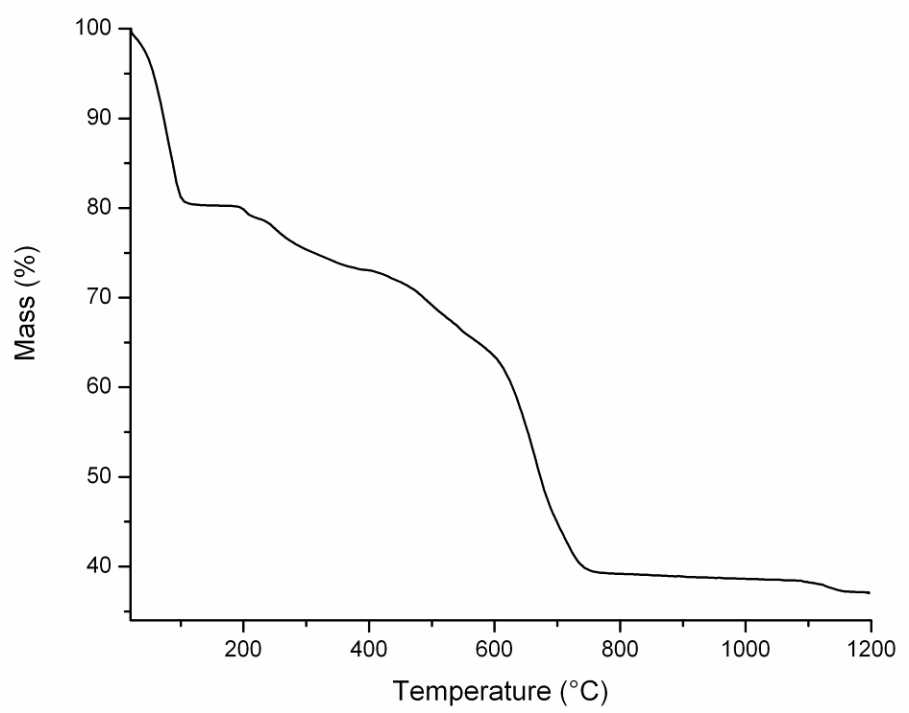

Figure S29. TG curve of **3**_ *lp**.

Gas Adsorpion Properties.

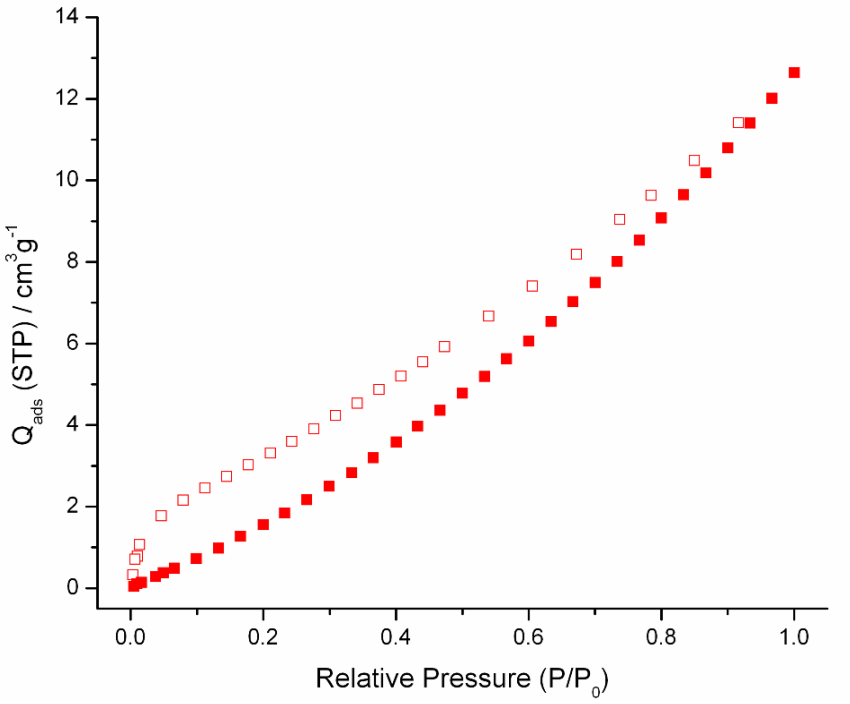

Figure S30. CO_2 adsorption (solid squares) and desorption (open squares) isotherms (195 K) measured for **1**.

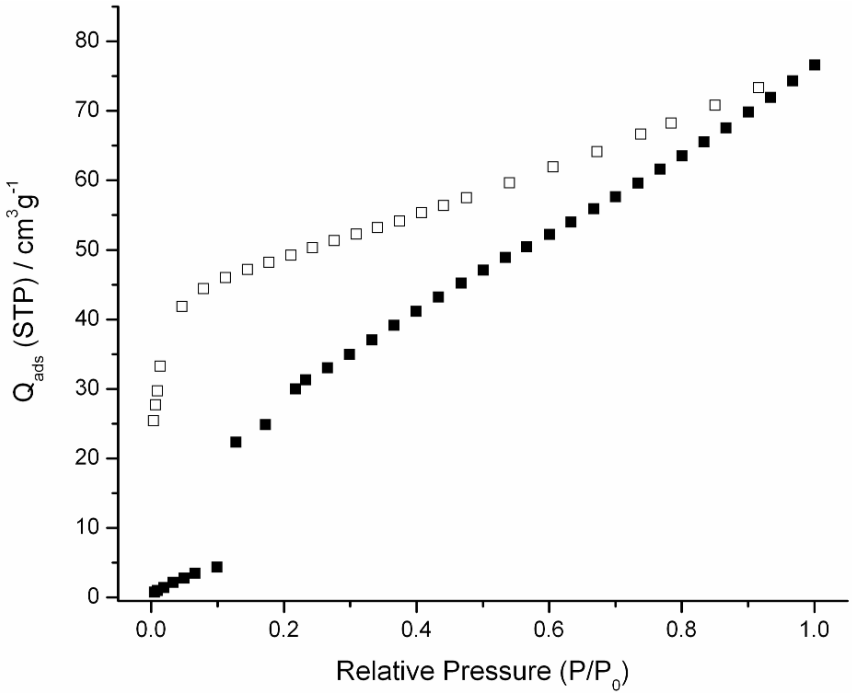

Figure S31. CO_2 adsorption (solid squares) and desorption (open squares) isotherms (195 K) measured for **2**.

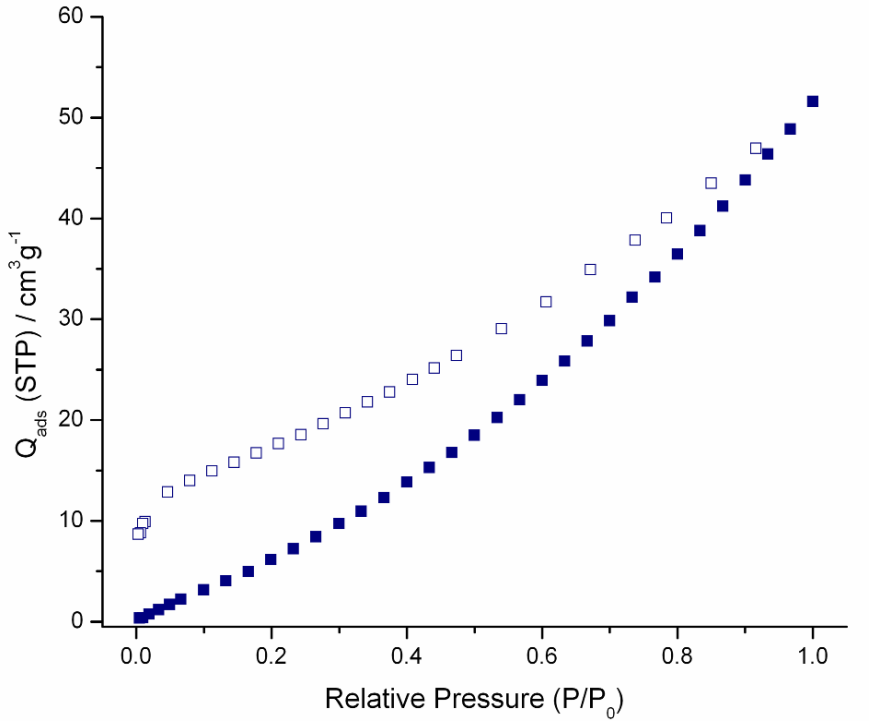

Figure S32. CO_2 adsorption (solid squares) and desorption (open squares) isotherms (195 K) measured for **3**.